Altruistic Resource-Sharing Mechanism for Synchronization: The Energy-Speed-Accuracy Trade-off

Dongliang Zhang (张东良),[1,2] Yuansheng Cao,[1] Qi Ouyang,[3] and Yuhai Tu[4,*]
[1]Department of Physics, Tsinghua University, Beijing 100084, China
[2]The State Key Laboratory for Artificial Microstructures and Mesoscopic Physics, School of Physics, Peking University, Beijing 100871, China
[3]Institute for Advanced Study in Physics, School of Physics, Zhejiang University, Hangzhou 310058, China
[4]IBM T. J. Watson Research Center, Yorktown Heights, New York 10598, USA

(Received 3 February 2025; accepted 20 June 2025; published 17 July 2025)

Synchronization among a group of active agents is ubiquitous in nature. Although synchronization based on direct interactions between agents described by the Kuramoto model is well understood, the other general mechanism based on indirect interactions among agents sharing limited resources are less known. Here, we propose a minimal thermodynamically consistent model for the altruistic resource-sharing (ARS) mechanism wherein resources are needed for an individual agent to advance but a more advanced agent has a lower competence to obtain resources. We show that while differential competence in ARS mechanism provides a negative feedback leading to synchronization it also breaks detailed balance and thus requires additional energy dissipation besides the cost of driving individual agents. By solving the model analytically, our study reveals a general trade-off relation between the total energy dissipation rate and the two key performance measures of the system: average speed and synchronization accuracy. For a fixed dissipation rate, there is a distinct speed-accuracy Pareto front traversed by the scarcity of resources: scarcer resources lead to slower speed but more accurate synchronization. Increasing energy dissipation eases this trade-off by pushing the speed-accuracy Pareto front outward. The connections of our work to realistic biological systems such as the KaiABC system in cyanobacterial circadian clock and other theoretical results based on thermodynamic uncertainty relation are also discussed.

DOI: 10.1103/snks-5fff

Introduction—Collective behaviors are ubiquitous in nature across different scales from coordinated motion of molecular motors to bacterial swarming to bird flocking [1–4]. Despite their diversity, these systems all share a common feature: they operate out of equilibrium and cost free energy, which are used to counter the effects of inevitable internal and external noise in order to sustain the collective order [5–8].

Synchronization of molecular systems [9–11] is a collective phenomenon critical for maintaining biological functions. Mechanistically, synchronization can be achieved by either direct or indirect interactions between individual molecular systems. In the KaiABC system for the circadian clock of cyanobacteria, both the direct and indirect interaction mechanisms may be at work. The direct interactions are carried out by monomer shuffling between the KaiC hexamers [10,12–17]; and the indirect interactions among KaiC hexamers are mediated by the shared pool of KaiA molecules, which are the key regulators for phosphorylation reactions that generate the circadian rhythm for KaiC hexamers [9,11,18–22].

In a previous work [6], we studied thermodynamics of the direct interaction mechanism for synchronization based on monomer shuffling of the KaiC hexamers, and discovered a trade-off relation between the energy cost and synchronization accuracy. In this Letter, we develop a thermodynamically consistent model to study the energy cost of the indirect interaction mechanism for synchronization inspired by KaiA differential binding in the KaiABC system (see Fig. 1 for an illustration of the two mechanisms). We find that the same energy-speed-accuracy relation holds as in the direct interaction mechanism, suggesting a universal relation between energy cost and synchronization performance independent of detailed mechanisms.

The altruistic resource-sharing model—We consider N agents each with a state variable x, and M resource molecules, which we call activators in this Letter as they activate the processive motion of agents. When bound with the activator, an agent can advance through a biased random walk process: the rate to step forward is k, and the rate to step backward is γk, where the ratio $\gamma = e^{-e_p \Delta x} < 1$ depends on the driving energy $e_p (> 0)$ for

*Present address: Center for Computational Biology & Center for Computational Neuroscience, Flatiron Institute, New York, New York 10010, USA.

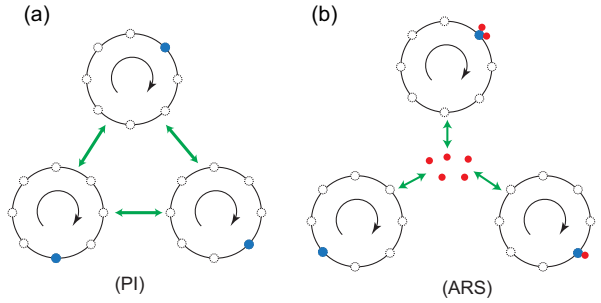

FIG. 1. Illustration of the two general synchronization mechanisms. The empty circles and filled circles represent all possible states and the current state in the oscillators (rings), respectively. (a) The local pair-wise interaction (PI) mechanism where the pair-wise interactions (green-arrowed lines) decrease the difference between the two interacting oscillators. (b) The global indirection interaction mechanism where the oscillators interact through sharing resources (red dots) needed for advancing the states of the oscillation. To achieve synchronization, the altruistic resource sharing (ARS) mechanism allows the lagger (the oscillator on the top) to gain more resources than the oscillators at the bottom that are more advanced.

the biased random walk per unit "length" (step). We let the "distance" between neighboring states $\Delta x = 1$ to set the scale for x. The slow diffusive motion of an activator-free agent is neglected in this work.

The binding and unbinding rate for the activator is q and $qe^{E(x)}$, respectively, where $E(x)$ is the binding energy for the agent with state variable x. In the altruistic resource-sharing mechanism, $E(x)$ increases with x, which creates an effective negative feedback to prevent leading ("rich") agents from getting more resources. In this study, we focus mainly on the case where the binding and unbinding reactions are much faster than the processive reactions, i.e., $q, qe^{E(x)} \gg k$ so that quasiequilibrium is valid for the binding and unbinding processes. As shown in Supplemental Material (SM) [23], finite values of q affect the transient dynamics without changing the steady-state behaviors.

The ARS mechanism works only when $E(x)$ is a monotonically increasing function of x. To understand details of how ARS leads to synchronization, we study the "linear" case where the state variable x can increase without bound. The role of ARS for synchronization for realistic oscillators with a periodic state variable will be discussed later in this Letter. For simplicity, we use a linear form for $E(x) = \alpha x$, where $\alpha > 0$ is the binding energy increase per unit length. A larger α indicates a larger affinity difference and stronger negative feedback. The effects of nonlinear $E(x)$ are discussed in SM [23].

The simplest case—To gain intuition about the dynamics and energetics of the altruistic resource-sharing (ARS) model, we first investigate the simplest case with two agents and one activator: $N = 2$, $M = 1$. Furthermore, we consider the situation $(e^{E(x)} \ll 1)$ where there is no unbound (free) activator.

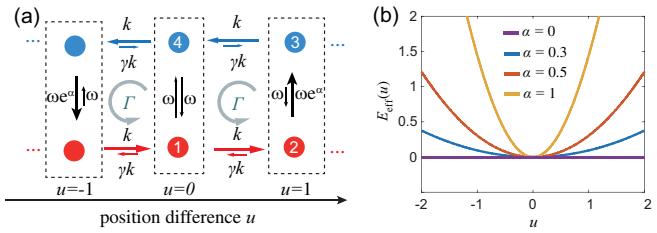

FIG. 2. Illustration of the simplest model $(M = 1, N = 2)$. (a) Dynamics of the system projected onto the u-axis. The red and blue dots represent the states where the activator is bound to either agent-1 or agent-2, respectively. ω represents a nominal rate for activator switching from one agent to the other. See text for detailed description. (b) The effective potential $E_{eff}(u)$ arises with finite $\alpha > 0$.

Synchronization can be evaluated by the difference between the two agents: $u \equiv x_1 - x_2$. Dynamics of the system projected onto the u axis is shown in Fig. 2(a), where the red and blue dotes represent the state where activator is bound either to agent-1 or agent-2, respectively. Starting from the synchronized state-1 where $u = 0$ and agent-1 is bound with the activator, the system goes to the asynchronized state-2 with $u = 1$ due to the processive motion of agent-1. Since agent-1 now has a larger x than agent-2 $(u = 1 > 0)$, it loses the activator to agent-2 with a high probability due to ARS and the system goes to state-3 where the activator is now bound with agent-2. Due to processive motion of agent-2, state-3 will then transition to state-4, which is again synchronized $(u = 0)$ as both agents have advanced by 1.

The combination of processive motion and the differential binding and unbinding reactions $(\alpha > 0)$ forms the dissipative flux cycle shown in Fig. 2(a), which can be quantified by the ratio between the products of rates in counterclockwise and clockwise directions:

$$\Gamma \equiv \frac{\prod_{ccw}(\text{rates})}{\prod_{cw}(\text{rates})} = \frac{e^{\alpha}}{\gamma^2} = e^{2e_p+\alpha}, \tag{1}$$

which shows that the system operates out of equilibrium $(\Gamma \neq 1)$ due to both directed motion $(e_p > 0)$ and differential affinity $(\alpha > 0)$.

Quantitatively, we can solve the Fokker-Planck equation for the joint probability density $P(x_1, x_2, t)$ in the continuum limit [24]:

$$\frac{\partial P}{\partial t} = -k \sum_{i=1}^{2} \frac{\partial}{\partial x_i} \left(e_p p_i P - \frac{\partial}{\partial x_i} p_i P \right), \tag{2}$$

where p_i is the probablity for the i th agent to be bound with the activator, which is given by $p_i = e^{-E(x_i)}/(e^{-E(x_1)} + e^{-E(x_2)})$. The first term reflects the directional drift due to biased random walk with activator bound, and the second term describes diffusion [see SM [23] for the

derivation of Eq. (2)]. We show that the average position $\bar{x} \equiv (x_1 + x_2)/2$ has a mean velocity $v = ke_p/2$ and the steady state distribution $P_s(u)$ of the difference u is given by (see SM for details [23])

$$P_s(u) = Z_2^{-1} \exp\left(-\frac{2e_p}{\alpha} \ln\cosh\frac{\alpha u}{2}\right), \tag{3}$$

where $Z_2 \equiv \int \exp\left[-(2e_p/\alpha)\ln\cosh(\alpha u/2)\right]\mathrm{d}u$ is the normalization constant. From $P_s(u)$, we can define an effective potential E_{eff}: $E_{eff}(u) \equiv -\ln(P_s(u)) = 2(e_p/\alpha)\ln\cosh(\alpha u/2)$. As shown in Fig. 2(b), $E_{eff}(u)$ is flat for $\alpha = 0$, and it has a minimum at $u = 0$ for $\alpha > 0$ and thus stabilizes the synchronized state.

The thermodynamic limit—In the thermodynamic limit $N \to \infty, M \to \infty$ with a finite $M/N \equiv A_t$, the state variable x of all agents at time t can be described by a probability density function $\rho(x,t)$. Dynamics of $\rho(x,t)$ satisfy the Fokker-Planck equation

$$\frac{\partial \rho(x,t)}{\partial t} = -k\frac{\partial}{\partial x}\left(e_p p(x)\rho - \frac{\partial}{\partial x} p(x)\rho\right), \tag{4}$$

where $p(x)$ is the probability of a agent with state variable x being bound to an activator. As detailed in SM [23] (including reference [25]), we can derive an expression for $p(x) = 1/[\mathrm{e}^{\alpha(x-x_0)} + 1]$ where x_0 is a normalization parameter determined by conservation of activators:

$$\int p(x)\rho(x,t)\mathrm{d}x = \int \frac{1}{\mathrm{e}^{\alpha(x-x_0)}+1}\rho(x,t)\mathrm{d}x = A_t. \tag{5}$$

Note that we have neglected free activators in Eq. (5) by assuming $e^{E(x)} \ll 1$ and $A_t < 1$. The effects of having a finite number of free activators are studied in SM [23].

Remarkably, Eqs. (4) and (5) can be solved analytically to obtain a steady-state traveling wave solution $\rho(x,t) = \rho_s(u)$ where $u = x - vt$ is the relative position. The average drift speed of the population $v = ke_pA_t$ is the product of the average speed (ke_p) of individual activator-bound (activated) agents and the fraction (A_t) of activated agents in the population. The analytical expression of $\rho_s(u)$ is (see SM for detailed derivation [23])

$$\rho_s(u) = \frac{1}{Z}(e^{\alpha u} + 1)\exp\left[e_p(1-A_t)u - \frac{A_t e_p}{\alpha}e^{\alpha u}\right], \tag{6}$$

where $A_t > 0$ describes the resource abundance relative to demand and Z is the normalization constant.

We use variance of u to characterize the synchronization performance: $\sigma^2 \equiv \int (u-\bar{u})^2\rho_s(u)\mathrm{d}u$ with $\bar{u} \equiv \int u\rho_s(u)\mathrm{d}u$. Smaller σ indicates better synchronization. Direct numerical simulations show that σ^2 decreases with α [Fig. 3(a)] but always saturates to a finite value σ_s^2 that increases with A_t [Fig. 3(a)]. This behavior can be understood from the analytical expression of the steady-state distribution $\rho_s(u)$ given in Eq. (6).

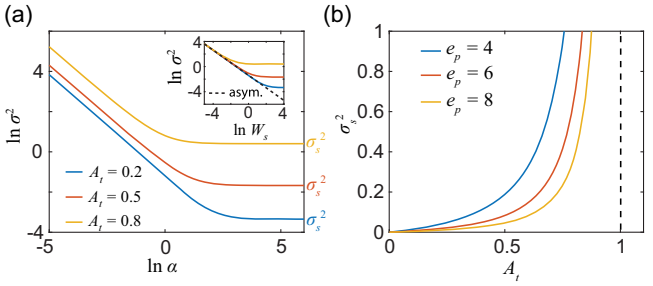

FIG. 3. Dependence of synchronization on key parameters. (a) The dependence of σ^2 on α with fixed $e_p = 8$ and different A_t. σ decreases with α and saturates to a finite value σ_s for large value of α. Inset: the dependence of σ^2 on dissipation W_s collapses onto the same curve for different values of A_t before saturation, consistent with the asymptotic expression Eq. (12) (dotted line). (b) The dependence of the saturation variance σ_s^2 on A_t for different e_p. $\sigma_s \to 0$ when $A_t \to 0$ and increases with A_t. $\sigma_s \to \infty$ when $A_t \to 1$ (dotted line).

In the weak sharing limit $\alpha \ll 1$, by expanding the effective potential $E_{\mathrm{eff}} \equiv -\ln(\rho_s)$ near its minimum, we have a leading order estimation for σ^2:

$$\sigma^2 \approx \frac{1}{\alpha e_p(1-A_t)}, \quad \alpha \ll 1, \tag{7}$$

which clearly shows that synchronization improves with increasing α and e_p in agreement with direct simulation results shown in Fig. 3(a).

In the strong sharing limit $\alpha \gg 1$, ρ_s becomes the sum of a δ-function distribution and an exponential distribution (see SM for details [23]):

$$\rho_{s,\infty}(u) = (1-A_t)\delta(u) + A_t\rho_e(u)H(-u), \tag{8}$$

where H is the Heaviside step function and $\rho_e(u) = \lambda \mathrm{e}^{\lambda u}$ with $\lambda = e_p(1-A_t)$. By using Eq. (8), we obtain an analytical expression of the saturation variance σ_s,

$$\sigma_s^2 \equiv \sigma^2(\alpha \to \infty) = \frac{(2-A_t)A_t}{e_p^2(1-A_t)^2}, \tag{9}$$

which diverges as $A_t = 1$ and becomes zero as $A_t = 0$; and it also decreases with the processive driving force e_p all consistent with numerical results shown in Fig. 3(b).

Besides the importance of differential binding ($\alpha > 0$), our results also reveal that synchronization depends critically on the relative resource abundance (A_t). Based on Eq. (7), the variance σ^2 diverges when $A_t \to 1$, which means that the ARS mechanism only works when the resource is relatively scarce ($A_t < 1$) and synchronization

improves as A_t decreases. The expression for $\rho_{s,\infty}(u)$ [Eq. (8)] reveals the surprising finding that the system is only partially synchronized even in the limit of infinite sharing ($\alpha \to \infty$). Indeed, Eq. (9) shows that the system only becomes perfectly synchronized in the limit of both $\alpha \to \infty$ and $A_t \to 0$.

The energy-speed-accuracy relation—Under the fast binding approximation, the free energy dissipation rate per agent can be computed by following previous work [26,27]:

$$\dot{W} \approx \int \frac{J^2}{kp\rho} \mathrm{d}\vec{x} = A_t k e_p^2 + k \int \frac{1}{p\rho} \left(\frac{\partial(p\rho)}{\partial x} \right)^2 \mathrm{d}\vec{x}, \quad (10)$$

where $J \equiv k e_p p\rho - k\partial_x(p\rho)$ is the processive probability flux. The first term in Eq. (10), denoted by $\dot{W}_0 = A_t k e_p^2 = v e_p$, is the dissipation for driving the processive dynamics of an individual agent. The second term, denoted by $\dot{W}_s$, is the dissipation for driving differential binding. Using expressions for $p(x)$ and $\rho_s(x)$, we have $\dot{W}_s = v(1 - A_t)\alpha$ (see SM for details [23]). Put together, the total dissipation can be written as

$$\dot{W} = \dot{W}_0 + \dot{W}_s = v e_p + v(1 - A_t)\alpha. \quad (11)$$

A new class of inequalities called the thermodynamic uncertainty relation (TUR), which relates entropy production with the mean and variance of an observed flux (current), have been used to set a lower bound for the dissipation based on the variance and average of an observable flux [28–31]. Following previous study on TUR for synchronized oscillators [30], we found that the TUR bound $\dot{W}_{TUR}$ obtained from statistics of a local flux does not provide an accurate estimate for the dissipation of the whole system $\dot{W}$ (see SM for details [23]).

Combining Eqs. (7), (9), and (11), we can quantitatively relate the free energy dissipation and the synchronization error given by σ^2:

$$\sigma^2 \approx \begin{cases} \frac{1}{W_s W_0}, & W_s \ll W_c, \\ \frac{(2-A_t)A_t}{W_0^2(1-A_t)^2}, & W_s \gg W_c, \end{cases} \quad (12)$$

where $W_s \equiv \dot{W}_s / v = (1 - A_t)\alpha$ and $W_0 \equiv \dot{W}_0 / v = e_p$ are the dissipation per unit length for driving synchronization and processive motion, respectively, and $W_c \equiv [(1 - A_t)^2 / A_t(2 - A_t)]W_0$ is a crossover dissipation.

Equation (12) clearly shows the trade-off between synchronization error and energy dissipation. The inverse σ^2-W_s dependence for different values of A_t collapse onto the same curve before they saturate beyond the crossover dissipation W_c, which decreases with A_t and increases with W_0 [see inset of Fig. 3(a)]. While synchronization is more accurate for lower resource abundance (smaller A_t) and stronger directed motion (larger e_p); the speed $v(= k_p A_t)$, which is the other important measure of the system's performance, increases with both e_p and A_t.

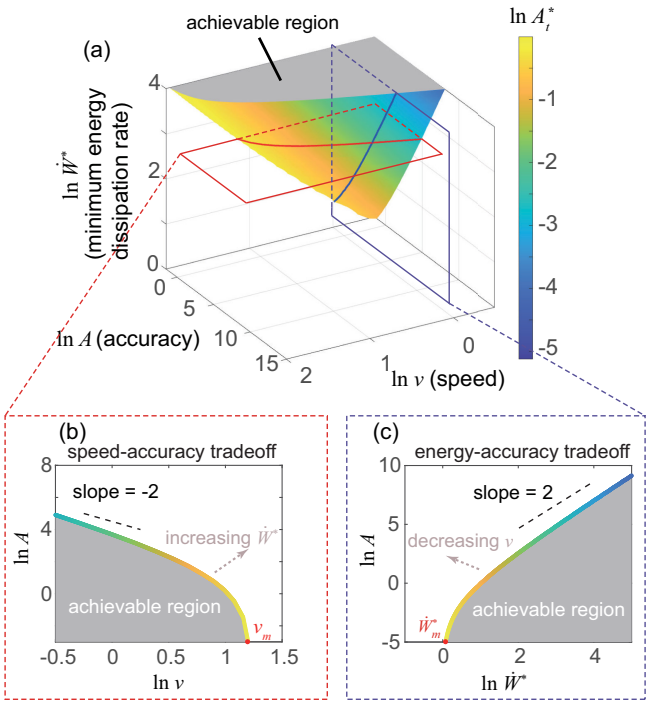

FIG. 4. The energy-speed-accuracy trade-off. (a) The Pareto surface, i.e., the minimum total energy dissipation rate $\dot{W}^*$ for given speed and accuracy (v, A). The color on the surface represents the optimal A_t^* to achieve the minimum $\dot{W}^*$. The gray volume is the achievable region in $(\dot{W}^*, v, A)$ space. (b) The trade-off between speed (v) and synchronization accuracy (A) with a fixed $\dot{W}^*$. The (v-A) Pareto front shifts outward with increasing $\dot{W}^*$. The maximum achievable speed for a fixed $\dot{W}^*$ is: $v_m = (k\dot{W}^*)^{1/2}$. (c) The trade-off between accuracy A and dissipation rate $\dot{W}^*$ with a fixed speed v. The minimum required dissipation for a desired speed v is $\dot{W}_m^* = v^2/k$.

By sweeping through the parameter space (A_t, e_p, α), we studied the minimum energy dissipation rate $\dot{W}^*$ for achieving a given system-level performance characterized by the synchronization accuracy A defined as $A \equiv \sigma^{-2}$ and the average speed v. As shown in Fig. 4(a), the 2D "Pareto" surface $\dot{W}^*(v, A)$ represents the energy-speed-accuracy (ESA) relationship: any performance (v, A) inside the Pareto surface is achievable with a minimum energy dissipation rate $\dot{W} \geq \dot{W}^*(v, A)$; performance outside the Pareto surface is forbidden. Each point $(\dot{W}^*, v, A)$ on the Pareto surface is achieved by an "optimal" set of parameters (A_t^*, e_p^*, α^*). In Fig. 4, the optimal A_t^* is represented by the color on the Pareto surface [32].

To understand the ESA trade-off, we dissect the ESA Pareto surface along different directions. In Fig. 4(b), we cut the Pareto surface at a fixed minimum dissipation, which shows a Pareto front in the performance space (v, A) that clearly demonstrates the accuracy-speed trade-off

modulated by the choice of A_t^* represented by the color along the Pareto front. As A_t^* changes along the Pareto front, the system goes from higher accuracy and lower speed at smaller A_t^* to lower accuracy and higher speed at larger A_t^*. For a fixed $\dot{W}^*$, there is a maximum speed $v_m = (k\dot{W}^*)^{1/2}$ at $A_t \to 1$ when all the energy is used for processive motion ($\dot{W}_0 \approx \dot{W}^*$); for $v \ll v_m$, we have $A \propto v^{-2}$. As we increase the minimum dissipation $\dot{W}^*$, the Pareto front moves outward, extending the achievable performance region. We can also cut the Pareto surface at a fixed speed v and plot the accuracy versus the minimum dissipation [Fig. 4(c)], which shows that there is a minimum dissipation $\dot{W}_m = v^2/k$ needed for achieving a finite accuracy. For $\dot{W}^* \gg \dot{W}_m$, we have $A \propto \dot{W}^{*2}$, and the higher accuracy is driven by a decreasing A_t^*.

The same dependence of synchronization error on energy dissipation as Eq. (12) is also found in the other general synchronization mechanism based on direct interactions between agents [6] (see SM for a detailed derivation [23]). Together, our results suggest that the ESA relation is universal in synchronization of molecular systems.

Discussion—In this work, we introduced a minimal model to study the altruistic resource-sharing (ARS) mechanism for synchronization with indirect agent-agent interaction. We showed that the ARS mechanism necessarily costs energy to facilitate differential binding critical for synchronization. The energy cost, the collective speed of the agents, and the accuracy of synchronization satisfy the same energy-speed-accuracy (ESA) trade-off relation found in the direct pairwise interacting (PI) mechanism studied previously [6], which suggest that the ESA relation for synchronization is independent of details of the underlying mechanisms. The robustness of the ESA relation is tested by introducing intrinsic variability for individual agents, i.e., quenched disorder in the system. While the quenched disorder lowers the speed and synchronization accuracy, the ESA relation hold true (see SM for details [23]). Remarkably, sensory adaptation systems [33] also exhibit a robust ESA relation independent of whether the underlying control mechanism is negative feedback [34] or incoherent feedforward [35]. The ESA relation reveals that increasing energy dissipation can ease the trade-off between key performance measures, e.g., speed and accuracy as shown in Fig. 4. Besides sensory adaptation [34,36], this general functional role of energy dissipation also applies to other nonequilibrium biological systems such as biochemical oscillation [37,38] and signal transduction [39,40].

Although they share the universal ESA relation, there are important differences between the ARS and PI mechanisms for synchronization. First, while the PI mechanism depends on direct interactions between agents, the ARS mechanism requires additional resource particles (activators) to mediate the indirect interactions between agents. In particular, differential binding of the agents to the activator ($\alpha > 0$) mediates an effective (indirect) interaction among agents that favors synchronization. Second, for the PI mechanism, the coupling between agents is introduced by additional chemical reactions with rates and strength that are independent of the processive dynamics of individual agents. However, for the ARS mechanism, the differential affinity of the resource (α) directly affects the processive dynamics of individual agents. As a result, the synchronization performance in ARS depends not only on α but also explicitly on the processivity of the agents characterized by e_p as shown by the expression of σ^2 given in Eqs. (7) and (9).

In this Letter, we demonstrate the ARS mechanism for synchronization by focusing on the "linear" case where the state variable changes without bound. For realistic oscillators with a periodic state variable, the ARS mechanism only works in part of the period. Can the ARS mechanism still lead to synchronization? We addressed this question by developing a simple model where the ARS mechanism can only function during half of the oscillation period when the phase $\phi \in [0, \pi]$ followed by unconstrained drift diffusion during the remaining half ($\phi \in [\pi, 2\pi]$). We found that synchronization occurs when the differential binding effect is larger than a critical value $\alpha > \alpha_c$. However, synchronization accuracy is lower than that of the linear case due to the uncontrolled phase diffusion when $\phi \in [\pi, 2\pi]$ (see SM for details [23], including reference [41]).

Many experiments suggest that the ARS mechanism applies in the KaiABC system [9,42–45]. In particular, the nucleotide exchange factor KaiA, which facilitates the successive phosphorylation of KaiC hexamer, has a higher affinity to the KaiC hexamers with a lower phosphorylation level [20,46]. Another evidence for the ARS mechanism is that the total KaiA concentration (A_t) plays an important role in controlling synchronization: a relatively low A_t is essential for synchronization, which is consistent with experiments that show the disappearance of coherent oscillation for high levels of KaiA [47,48]. However, the ARS mechanism functions only during the phosphorylation phase (subjective day) of the KaiABC circadian cycle. On the other hand, monomer shuffling between KaiC hexamers, an observed phenomenon [10,12,14–17], can also contribute to synchronization through the PI mechanism [6,13]. Interestingly, monomer shuffling occurs more frequently during the dephosphorylation phase (subjective night) [14]. Taken together, these observations present an exciting opportunity to explore how these two mechanisms may work together during the full circadian cycle to achieve precise synchronization efficiently in the KaiABC system.

Resource sharing is an ubiquitous phenomenon in living systems across all scales. For example, resource sharing is critical in driving cooperative behaviors in ecology and evolution [49,50]. Here, we showed how altruistic resource sharing (ARS) can lead to synchronization in molecular systems. The two key ingredients of ARS, the limited resource and differential affinity, are also present in various

other molecular systems, such as bacterial DNA replication initiation [51,52] and combinatorial signal processing in the BMP pathway [53–56]. It would be interesting to test if similar cost-performance trade-off relation as the ESA relation for synchronization could be found in these systems.

Acknowledgments—The work of Y. T. was supported by an NIH grant (R35GM131734) when Y. T. worked for IBM Research. The Flatiron Institute, where Y. T. is currently employed, is a division of the Simons Foundation. The work of Q. O. is supported by the Starry Night Science Fund of Zhejiang University Shanghai Institute for Advanced Study. The work of D. Z. and Y. C. is supported by the National Natural Science Foundation of China (Grants No. 12090054 and No. 12374213). We would like to thank the anonymous referees for constructive comments that have improved the Letter. D. Z. would like to thank his current institute, the Max Planck Institute for the Physics of Complex Systems (MPIPKS), for hospitality and support during revision of this Letter. D. Z. would also like to thank Shiling Liang and other colleagues at MPIPKS for useful discussions.

Data availability—No data were created or analyzed in this study.

[1] M. C. Marchetti, J.-F. Joanny, S. Ramaswamy, T. B. Liverpool, J. Prost, M. Rao, and R. A. Simha, Rev. Mod. Phys. **85**, 1143 (2013).
[2] W. Bialek, A. Cavagna, I. Giardina, T. Mora, E. Silvestri, M. Viale, and A. M. Walczak, Proc. Natl. Acad. Sci. U.S.A. **109**, 4786 (2012).
[3] J. Toner and Y. Tu, Phys. Rev. E **58**, 4828 (1998).
[4] J. Elgeti, R. G. Winkler, and G. Gompper, Rep. Prog. Phys. **78**, 056601 (2015).
[5] Q. Yu and Y. Tu, Phys. Rev. Lett. **129**, 278001 (2022).
[6] D. Zhang, Y. Cao, Q. Ouyang, and Y. Tu, Nat. Phys. **16**, 95 (2020).
[7] J. A. Acebrón, L. L. Bonilla, C. J. Pérez Vicente, F. Ritort, and R. Spigler, Rev. Mod. Phys. **77**, 137 (2005).
[8] J. Tailleur, G. Gompper, M. C. Marchetti, J. M. Yeomans, and C. Salomon, *Active Matter and Nonequilibrium Statistical Physics: Lecture Notes of the Les Houches Summer School, 2018* (Oxford University Press, New York, 2022), Vol. 112.
[9] J. S. van Zon, D. K. Lubensky, P. R. Altena, and P. R. ten Wolde, Proc. Natl. Acad. Sci. U.S.A. **104**, 7420 (2007).
[10] T. Nagai, T. P. Terada, and M. Sasai, Biophys. J. **98**, 2469 (2010).
[11] J. Paijmans, D. K. Lubensky, and P. R. ten Wolde, PLoS Comput. Biol. **13**, e1005415 (2017).
[12] H. Kageyama, T. Nishiwaki, M. Nakajima, H. Iwasaki, T. Oyama, and T. Kondo, Mol. Cell **23**, 161 (2006).
[13] E. Emberly and N. S. Wingreen, Phys. Rev. Lett. **96**, 038303 (2006).
[14] H. Ito, H. Kageyama, M. Mutsuda, M. Nakajima, T. Oyama, and T. Kondo, Nat. Struct. Mol. Biol. **14**, 1084 (2007).
[15] T. Mori, D. R. Williams, M. O. Byrne, X. Qin, M. Egli, H. S. Mchaourab, P. L. Stewart, and C. H. Johnson, PLoS Biol. **5**, e93 (2007).
[16] M. Yoda, K. Eguchi, T. P. Terada, and M. Sasai, PLoS One **2**, e408 (2007).
[17] K. Eguchi, M. Yoda, T. P. Terada, and M. Sasai, Biophys. J. **95**, 1773 (2008).
[18] M. J. Rust, J. S. Markson, W. S. Lane, D. S. Fisher, and E. K. O'shea, Science **318**, 809 (2007).
[19] L. Ma and R. Ranganathan, PLoS One **7**, e42581 (2012).
[20] J. Lin, J. Chew, U. Chockanathan, and M. J. Rust, Proc. Natl. Acad. Sci. U.S.A. **111**, E3937 (2014).
[21] A. K. Behera, C. d. Junco, and S. Vaikuntanathan, J. Phys. Chem. B **125**, 11179 (2021).
[22] T. Mori, S. Sugiyama, M. Byrne, C. H. Johnson, T. Uchihashi, and T. Ando, Nat. Commun. **9**, 3245 (2018).
[23] See Supplemental Material at http://link.aps.org/supplemental/10.1103/snks-5fff for detailed derivations, comparison with the pairwise interaction mechanism, discussion regarding the thermodynamic uncertainty relation, discussion of the approximation in the model, the effect of quenched order, and the application to realistic oscillators.
[24] We did rescaling $k(\Delta x)^2 \to k$ in the continuum limit.
[25] F. Reif, *Fundamentals of Statistical and Thermal Physics* (McGraw-Hill, New York, 1965).
[26] T. Tomé and M. J. de Oliveira, Phys. Rev. E **82**, 021120 (2010).
[27] D. Zhang and Q. Ouyang, Entropy **23**, 271 (2021).
[28] A. C. Barato and U. Seifert, Phys. Rev. Lett. **114**, 158101 (2015).
[29] J. M. Horowitz and T. R. Gingrich, Nat. Phys. **16**, 15 (2020).
[30] S. Lee, C. Hyeon, and J. Jo, Phys. Rev. E **98**, 032119 (2018).
[31] C. Dieball and A. Godec, Phys. Rev. Lett. **130**, 087101 (2023).
[32] e_p^* and α^* can be determined from A_t^* and the targeted performance (v, A).
[33] Y. Tu and W.-J. Rappel, Annu. Rev. Condens. Matter Phys. **9**, 183 (2018).
[34] G. Lan, P. Sartori, S. Neumann, V. Sourjik, and Y. Tu, Nat. Phys. **8**, 422 (2012).
[35] G. Lan and Y. Tu, J. R. Soc. Interface **10**, 20130489 (2013).
[36] P. Sartori and Y. Tu, Phys. Rev. Lett. **115**, 118102 (2015).
[37] Y. Cao, H. Wang, Q. Ouyang, and Y. Tu, Nat. Phys. **11**, 772 (2015).
[38] C. Fei, Y. Cao, Q. Ouyang, and Y. Tu, Nat. Commun. **9**, 1434 (2018).
[39] D. Hathcock, Q. Yu, B. A. Mello, D. N. Amin, G. L. Hazelbauer, and Y. Tu, Proc. Natl. Acad. Sci. U.S.A. **120**, e2303115120 (2023).
[40] D. Hathcock, Q. Yu, and Y. Tu, Nat. Commun. **15**, 8892 (2024).
[41] J. A. Acebrón, L. L. Bonilla, C. J. P. Vicente, F. Ritort, and R. Spigler, Rev. Mod. Phys. **77**, 137 (2005).
[42] H. Takigawa-Imamura and A. Mochizuki, J. Bio. Rhythm. **21**, 405 (2006).
[43] S. Clodong, U. Dühring, L. Kronk, A. Wilde, I. Axmann, H. Herzel, and M. Kollmann, Mol. Syst. Biol. **3**, 90 (2007).

[44] F. Miyoshi, Y. Nakayama, K. Kaizu, H. Iwasaki, and M. Tomita, J. Bio. Rhythm. **22**, 69 (2007).
[45] I. M. Axmann, S. Legewie, and H. Herzel, Genome. Informatics **18**, 54 (2007).
[46] L. Ma and R. Ranganathan, PLoS One **7**, e42581 (2012).
[47] M. Nakajima, H. Ito, and T. Kondo, FEBS Lett. **584**, 898 (2010).
[48] A. G. Chavan, J. A. Swan, J. Heisler, C. Sancar, D. C. Ernst, M. Fang, J. G. Palacios, R. K. Spangler, C. R. Bagshaw, S. Tripathi *et al.*, Science **374**, eabd4453 (2021).
[49] M. B. Bonsall and A. E. Wright, Ecol. Evol. **2**, 515 (2012).
[50] J. J. Kreider, T. Janzen, A. Bernadou, D. Elsner, B. H. Kramer, and F. J. Weissing, Nat. Commun. **13**, 7232 (2022).
[51] M. L. Mott and J. M. Berger, Nat. Rev. Microbiol. **5**, 343 (2007).
[52] H. Fu, F. Xiao, and S. Jun, PRX Life **1**, 013011 (2023).
[53] Y. E. Antebi, J. M. Linton, H. Klumpe, B. Bintu, M. Gong, C. Su, R. McCardell, and M. B. Elowitz, Cell **170**, 1184 (2017).
[54] C. J. Su, A. Murugan, J. M. Linton, A. Yeluri, J. Bois, H. Klumpe, M. A. Langley, Y. E. Antebi, and M. B. Elowitz, Cell Syst. **13**, 408 (2022).
[55] H. E. Klumpe, M. A. Langley, J. M. Linton, C. J. Su, Y. E. Antebi, and M. B. Elowitz, Cell Syst. **13**, 388 (2022).
[56] H. E. Klumpe, J. Garcia-Ojalvo, M. B. Elowitz, and Y. E. Antebi, Cell Syst. **14**, 430 (2023).